SEISMIC RELIABILITY-BASED DESIGN OF STRUCTURES EQUIPPED WITH DFPS

Available online at www.easdprocedia.org
EASD Procedia EURODYN (2020) 3744-3761

EASD Procedia

EURODYN 2020
XI International Conference on Structural Dynamics
M. Papadrakakis, M. Fragiadakis, C. Papadimitriou (eds.)
Athens, Greece, 23–26 November 2020

SEISMIC RELIABILITY-BASED DESIGN OF STRUCTURES EQUIPPED WITH DFPS

P. Castaldo[1] **and G. Alfano**[2]

[1] Department of Structural, Geotechnical and Building Engineering (DISEG), Politecnico di Torino
Turin, Italy
e-mail: paolo.castaldo@polito.it

[2] Department of Political and Communication Sciences, University of Salerno, Via Giovanni Paolo 132, 84084 Salerno, Italy
e-mail: galfano@unisa.it

Keywords: seismic isolation, double friction pendulum bearing, seismic reliability-based design, ductility demand, behaviour factor, post-yield hardening/softening stiffness.

Abstract. *This work deals with seismic reliability-based design (SRBD) for softening and hardening structures equipped with double friction pendulum system (DFPS) isolators. The isolated system is represented by means of an equivalent 3dof model having a softening/hardening post-yield slope for the superstructure and velocity-dependent rules for the two surfaces of the DFP devices. The yielding characteristics of the superstructures are defined in compliance with the seismic hazard of L'Aquila site (Italy) and with NTC18 assuming ordinary characteristics. Considering several natural seismic records and the relevant random variables, incremental dynamic analyses are carried out for assessing the seismic fragility and the seismic reliability of these systems. Finally, seismic reliability-based design (SRBD) curves for these systems are proposed.*

ISSN:2311-9020
Peer-review under responsibility of the Organizing Committee of EURODYN 2020.
doi: 10.47964/1120.9307.20046

1 INTRODUCTION

Sliding pendulum bearings are more and more used to isolate buildings and infrastructures in seismic zone [1]-[3] and have been studied by many researchers (e.g., [4]-[5]) in order to ensure appropriate safety and resilience levels to infrastructure systems [6]-[7]. Probabilistic analyses together with reliability-based investigations have also been developed by [8]-[9] as well as reliability and reliability-based optimization analyses for base-isolated systems have been discussed in [10]-[11]. Adopting the friction coefficient in addition to the earthquake characteristics as the main aleatory uncertainties, seismic reliability and life-cycle cost analyses of 3D base-isolated reinforced concrete (RC) structures have been commented in [12]-[13]. Referring to elastic systems isolated through single FPS, the seismic reliability-based design (SRBD) approach in general terms has been presented in [14]. In the literature articles [15] and [16], two different optimization approaches are proposed for systems equipped with FPS: in [15], with the purpose to minimize the superstructure displacement demand, the influence of the system properties and of the soil conditions on the optimal friction coefficients is examined; in [16], the ratio peak ground acceleration/velocity is assumed as the relevant parameter to determine the optimal friction coefficients. The studies [17]-[19] investigated the seismic performance of bridges or structures equipped with DFPS (doubleFPS) or FPS providing [19] useful relationships to assess the seismic response of structures isolated by frictional isolators and highlighting that the principal benefit of the DFPS bearing in comparison to the singleFP is the capacity to accommodate larger displacements.

With regard to the design of base-isolated systems when they respond inelastically, seismic code provisions [20]-[24] prescribe low values for the strength reduction factor [20],[24] or behavior factor [21]-[22] to avoid non linear dynamic amplification phenomena (e.g., partial resonance) [25]. In detail, NTC18 [22], the Japanese building code [23] and Eurocode 8 [21] state 1.5 as maximum value, without specifying a distinction between the ductility and overstrength factor term. A behavior factor equal to 0.375 times the value for corresponding fixed-base structures and no larger than 2 is prescribed in ASCE 7 [20].

This study describes the seismic reliability-based design (SRBD) for softening and hardening structural systems equipped with DFPS devices and located in L'Aquila (Italy). The isolated system is represented by means of an equivalent 3-degree-of-freedom (3dof) model having a softening/hardening post-yield slope for the superstructure and velocity-dependent rules for the two surfaces of the DFP devices [4]. In this way, a wide parametric analysis is developed investigating the influence of different elastic and inelastic structural system properties of the superstructure and of the DFPS for increasing behavior factors [20]-[23]. In addition, the investigation is carried out assuming the both friction coefficients of the two surfaces of the DFPS and the characteristics of the ground motions as the main aleatory uncertainties. In detail, the both friction coefficients are modelled by means of appropriate Gaussian probability density functions (PDFs) and, the Latin Hypercube Sampling (LHS) method [26]-[27] is employed to generate the input data. After that, several incremental dynamic analyses (IDAs) are developed for increasing seismic intensity levels in compliance with the site seismic hazard to assess the seismic fragility curves and, successively, the seismic reliability curves. Finally, SRBD curves for the two surfaces of the DFPS devices are provided as design relationships. The results herein presented allow a comparison with the outcomes when single-FPS are employed [28],[29] in order to highlight the potential advantages of the DFPS and recommend reliable values of the displacement demands to the DFPS bearings.

2 EQUATIONS OF MOTION FOR NON-LINEAR STRCTURAL SYSTEMS WITH DFPS

The equivalent system depicted in Figure 1 is a 3dof system presents a dof for the superstructure behaviour and two dofs for the responses of the two surfaces of the DFPS. This equivalent system has been adopted to model the mechanical nonlinearities of the superstructure and of the DFPS [30].

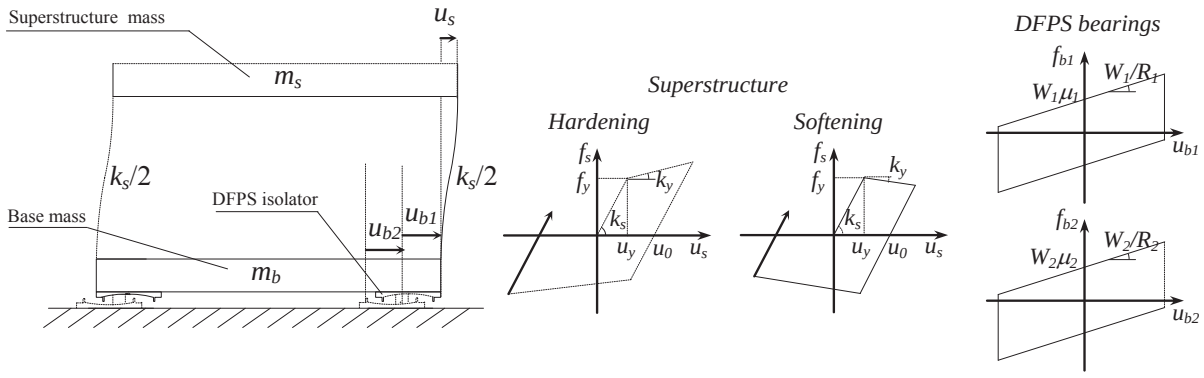

Figure 1: 3dof model with the constitutive laws.

Regarding the free body diagram of the DFPS, the bearing restoring forces of the DFPS apply:

$$f_{b,1} = \frac{W_1}{R_1} u_{b,1} + \mu_{d,1} W_1 \operatorname{sgn}\left(\dot{u}_{b,1}\right) \tag{1a}$$

$$f_{b,2} = \frac{W_2}{R_2} u_{b,2} + \mu_{d,2} W_2 \operatorname{sgn}\left(\dot{u}_{b,2}\right) \tag{1b}$$

where $W_1 = \left(m_b + m_s\right) g$ denotes the weight on the upper surface (surface 1) of the isolator, $W_2 = \left(m_b + m_s + m_d\right) g$ is the weight on the lower surface (surface 2) of the isolator, g is the gravity constant, R_1 and R_2 are the curvature radii of the two surfaces of the isolator, $u_{b,1}$ represents the displacement of the surface 1 with respect to the slider, $u_{b,2}$ is the slider displacement with respect to the ground, $\mu_{d,1}$ and $\mu_{d,2}$ denote the sliding friction coefficients of the two surfaces and sgn is the signum function of the sliding velocity for each surface. In this work, the surface 1 presents higher values of both the friction coefficient and the radius of curvature. Precisely, $\mu_{d,1}$ is chosen as $4\mu_{d,2}$ and $R_1=2R_2$ [30].

Along each surface, the friction coefficient applies [4]-[5]:

$$\mu_{d,i} = f_{\max,i} - \left(f_{\max,i} - f_{\min,i}\right) \exp\left(-\alpha \dot{u}_{b,i}\right) \quad \text{for } i = 1,2 \tag{2}$$

where $f_{\max,i}$ and $f_{\min,i}$ are, respectively, the friction coefficients at high and very low sliding velocities of the i-th surface. The values of 30 and 3 are assumed, respectively, for α and $f_{\max,i} / f_{\min,i}$ for each sliding surface [15],[28].

The hardening or softening behaviour of the superstructure is modelled herein through a bilinear constitutive law. In this way, the response is elastic if Eqn.(3) is verified and the restoring force $f_{s,i}$ is expressed according to Eqn.(4):

$$\left|u_{s,i}-u_{0,i-1}\right|<y\left(u_{s,i}\right) \tag{3}$$

$$f_{s,i}\left(u_{s,i}\right)=k_s\left(u_{s,i}-u_{0,i-1}\right) \tag{4}$$

where $f_{s,i}$ denotes the restoring force at time instant i, $u_{s,i}$ represents the superstructure deformation at the same instant, $u_{0,i-1}$ is the maximum inelastic response at time instant $(i-1)$ and k_s is the superstructure elastic stiffness. The term $y(u_{s,i})$ is the yielding function depending on the displacement as explained in [31]. Defining u_y as the yield displacement, whose yield force is f_y, H or S denotes the ratio of the hardening or softening post-yield stiffness over the elastic stiffness [32]-[33], evaluated as:

$$H=S=\frac{k_y}{k_s} \tag{5}$$

The superstructure response is in plastic phase if Eqn.(6) is verified and the restoring force can be calculated through Eqn.(7):

$$\left|u_{s,i}-u_{0,i-1}\right|\geq y(u_{s,i}) \tag{6}$$

$$f_{s,i}\left(u_s\right)=k_s(u_{s,i}-y(u_{s,i}))\,\mathrm{sgn}(u_{s,i}-u_{0,i-1}) \tag{7}$$

Therefore, the equations of motion that govern the inelastic response of the equivalent 3dof system to the seismic input $\ddot{u}_g(t)$, without any viscous dissipative capacities for the DFPS, are:

$$m_s\ddot{u}_s+(m_s+m_b)\ddot{u}_{b,1}+(m_s+m_b+m_d)\ddot{u}_{b,2}+\frac{W_2}{R_2}u_{b,2}+W_2\mu_2\,\mathrm{sgn}\left(\dot{u}_{b,2}\right)=-(m_s+m_b+m_d)\ddot{u}_g$$

$$m_s\ddot{u}_s+(m_s+m_b)\ddot{u}_{b,1}+(m_s+m_b)\ddot{u}_{b,2}+(m_s+m_b)\frac{g}{R_1}u_{b,1}+(m_s+m_b)g\mu_1\,\mathrm{sgn}\left(\dot{u}_{b,1}\right)=-(m_s+m_b)\ddot{u}_g$$

$$m_s\ddot{u}_s+m_s\ddot{u}_{b,1}+m_s\ddot{u}_{b,2}+c_s\dot{u}_s+f_{s,i}(u_s)=-m_s\ddot{u}_g \tag{8a,b,c}$$

where m_s, m_b and m_d represent respectively the mass of the superstructure, of the isolation level and of the slider, c_s is the superstructure viscous damping factor. Dividing Eqn.(8a) by $m_s+m_b+m_d$ as well as Eqn.(8b) by m_b+m_s and Eqn.(8c) by m_s, defining the mass ratios as $\gamma_s=m_s/(m_s+m_b+m_d)$, $\gamma_b=m_b/(m_s+m_b+m_d)$ and $\gamma_d=m_d/(m_s+m_b+m_d)$ [34], the isolation $\omega_{b,i}=\sqrt{g/R_i}$ and structural $\omega_s=\sqrt{k_s/m_s}$ circular frequency, the structural damping ratio $\xi_s=c_s/2m_s\omega_s$, the non-dimensional equations become as follows:

$$\gamma_s \ddot{u}_s + (\gamma_s + \gamma_b)\ddot{u}_{b,1} + \ddot{u}_{b,2} + \omega_{b,2}^2 u_{b,2} + g\mu_2 \operatorname{sgn}\left(\dot{u}_{b,2}\right) = -\ddot{u}_g$$
$$\gamma_s \ddot{u}_s + (\gamma_s + \gamma_b)\ddot{u}_{b,1} + (\gamma_s + \gamma_b)\ddot{u}_{b,2} + (\gamma_s + \gamma_b)\omega_{b,1}^2 u_{b,1} + (\gamma_s + \gamma_b) g\mu_1 \operatorname{sgn}\left(\dot{u}_{b,1}\right) = -(\gamma_s + \gamma_b)\ddot{u}_g$$
$$\ddot{u}_s + \ddot{u}_{b,1} + \ddot{u}_{b,2} + 2\omega_s \xi_s \dot{u}_s + a_s(u_s) = -\ddot{u}_g \tag{9a,b,c}$$

where $a_s\left(u_s\right) = f_s\left(u_s\right)/m_s$ denotes the dimensionless superstructure force proportional to the elastic stiffness k_s if the response is elastic or depends on the yielding condition if the system responds inelastically. Note that the elastic vibration period of the isolation system provided by the DFPS devices depends on which surfaces are moving during the earthquake [19]. In detail, if only one surface slides, the isolation period depends only on the radius of curvature of that surface R_i and the bearing behaves like a simple FPS [14], whereas when the both surfaces slide, the isolation effective period applies [19]:

$$T_b = 2\pi\sqrt{\frac{R_1 + R_2}{g}} \tag{10}$$

It follows that the seismic isolation degree [35], expressed as the variable isolation period over the structural period of vibration, is not a constant during an earthquake event. Moreover, when the both surfaces slide simultaneously the restoring force of the DFPS isolator can be evaluated as $\mu_e W_1$ neglecting the mass of the slider [30], where μ_e is the effective sliding coefficient given by:

$$\mu_e = \frac{\mu_{d,1} R_1 + \mu_{d,2} R_2}{R_1 + R_2} \tag{11}$$

Regards the inelastic behavior of the superstructure [36]-[37], Eqn.s (12)-(13) define, respectively, the inelastic capacities in terms of behavior factor, q, and displacement ductility, μ, defined, respectively, as:

$$q = \frac{f_{s,el}}{f_y} = \frac{u_{s,el}}{u_y} \tag{12}$$

$$\mu = \frac{u_{s,\max}}{u_y} \tag{13}$$

where $f_{s,el}$ and $u_{s,el}$ represent the peak response values, respectively, in terms of strength and displacement when the superstructure responds elastically during a ground motion, whereas $u_{s,\max} = \left|u_s(t)\right|_{\max}$ denotes the peak inelastic response in terms of displacement. The terms u_y and f_y are, respectively, the yielding displacement and strength. More details may be found in [30].

3 INCREMENTAL DYNAMIC ANALYSES

This section describes the results achieved from the incremental dynamic analyses (IDAs) of the system in Figure 1 within a wide parametric analysis, considering several structural parameters and as Italian site: L'Aquila (42°38'49''N and 13°42'25''E and a soil class B). In detail, the responses of the superstructure, of the DFPS are investigated for increasing intensity measure (*IM*) levels and shown in the following figures adopting 30 real ground motions,

which have also been used in previous studies by the authors [28],[29],[30], to describe the aleatory uncertainty on the seismic input denoted as record-to-record variability. The *IM* is herein chosen as the spectral displacement at the effective isolated period $S_D(T_b)$.

Elastic and inelastic properties of the isolated superstructure

Within the parametric analysis, the following deterministic parameters are taken into account: the isolation degree I_d with respect to the equivalent effective isolated period of Eq.(10) = 2, 4, 6 and 8; the equivalent effective isolation period T_b of Eq.(10) = 3s, 4s, 5s and 6s; the mass ratios: γ_s = 0.6 and 0.8, γ_d = 0.001, and so γ_b = 0.399 and 0.199; the behaviour factor q = 1.1, 1.2, 1.3, 1.4, 1.5, 1.6, 1.7, 1.8, 1.9 and 2, according to [20]-[23], and the post-yield softening or hardening stiffness ratio S or H = 0.03 [38]-[39]. Combing all these properties, 768 equivalent inelastic 3dof systems derive. The isolation damping ratio ξ_b is assumed equal to 0% whereas, superstructure damping ratio ξ_s equal to 2%.

Neglected the inelastic properties and considering only the elastic ones, 32 different 3dof systems derive (with the different values of I_d, of T_b and of the mass ratios). Assuming $\mu_{d,1}$ and $\mu_{d,2}$ equal to 4% and 1%, respectively, and a ratio equal to 2 between R_1 and R_2 [30], for 32 elastic 3dof elastic systems, it has been possible to evaluate the average elastic responses, in Matlab-Simulink [40], to the 30 records scaled to the *IM* value of the life safety limit state for L'Aquila: the $IM = S_D(T_b)$ applies 0.311 m for T_b=3, 4, 5 s and 0.26 m for T_b =6 s [22]. In this way, the yielding characteristics of the 768 inelastic 3dof systems have been computed in terms of the average values of both yield strength and yield displacement (i.e., $f_{y,\text{average}}$ and $u_{y,\text{average}}$) divided by the increasing values of q, as expressed by Eqn.(14):

$$u_{y,average} = \frac{f_{y,average}}{k_s} = \frac{f_{s,el,average}}{k_s q} = \frac{u_{s,el,average}}{q} \tag{14}$$

Incremental dynamic analysis (IDA) curves

This sub-section deals with the responses of the 768 equivalent 3dof hardening and softening systems, considering the aleatory uncertainties of the sliding friction coefficients through 15 sampled couples, to the 30 seismic inputs scaled to the increasing $IM = S_D(T_b)$, varying in the range from 0 m to 0.45 m. Specifically, for each *IM* level and parameter combination, 450 numerical non-linear analyses have been developed. The isolated non-linear hardening and softening systems are modelled in Matlab-Simulink [40], by employing the Runge-Kutta-Fehlberg integration algorithm to solve Eqn.(9) and determine the responses of the superstructure and of the DFPS bearings.

For each softening structural system, the collapse condition assumed within the numerical analyses is reached when the response of the superstructure is equal to zero. For the other systems as well as for the isolation devices any limitation is not considered.

Form the results of the non-linear incremental dynamic analyses, it has been possible to estimate the collapsed system cases together with the displacement ductility demand μ for the superstructure and the displacements for the DFPS (i.e., peak value for each one of the two surfaces "$u_{b,1}$ and $u_{b,2}$" and peak value of their sum computed at each time instant "u_b"). These response parameters are denoted as the engineering demand parameters (EDPs) and their peak

values have been fitted by means of lognormal distributions [12]-[15],[28],[41],[42] at each *IM* level. In detail, for each lognormal distribution, through the maximum likelihood estimation (MLE) technique [43]-[47], the mean, $\mu_{\ln}(EDP)$, and the standard deviation, $\sigma_{\ln}(EDP)$, have been computed as well as the 50th, 84th and 16th percentile.

It is also important to specify that neither other aleatory uncertainties not epistemic uncertainties have been herein considered [48]-[49].

Figures 2-3 depict the IDA curves for hardening structures. The results related to I_d =2 and 8, T_b =3s and 6s and γ_s equal to 0.6 are herein illustrated.

Fig. 2 depicts the IDA curves of the isolation level EDP $u_{b,\max}$, which is the peak value of the sum of $u_{b,1}$ and $u_{b,2}$ in each time instant. The lognormal mean of $u_{b,\max}$ is higher by increasing T_b and I_d. Moreover, the increase of q causes a slight decrease of $u_{b,\max}$, especially for higher values of I_d. The results are consistent with the ones achieved in [29] considering a single concave sliding device.

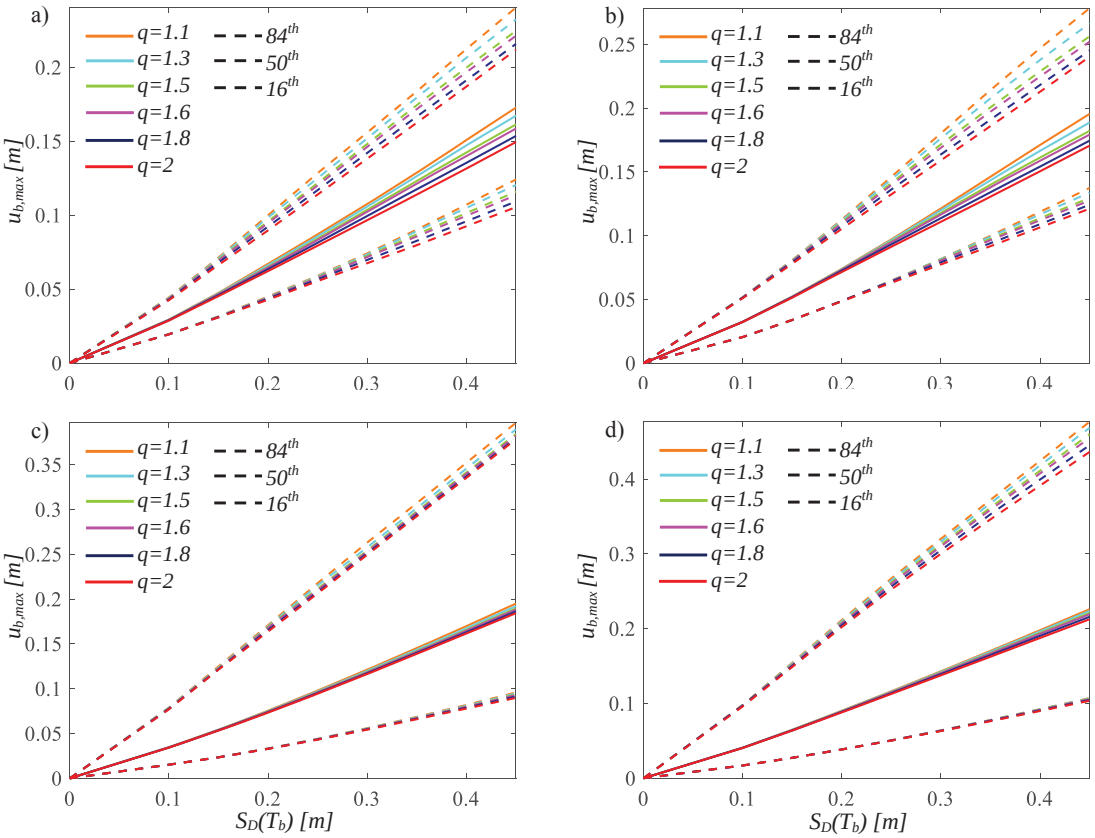

Figure 2: IDA curves of the isolation level with γ_s =0.6 for I_d=2, T_b=3 s, H=0.03 (a), I_d=2, T_b=6 s, H=0.03 (b), I_d=8, T_b=3 s, H=0.03 (c), I_d=8, T_b=6 s, H=0.03 (d).

Fig. 3 depicts the IDA results for the EDP μ. The corresponding statistical parameters are strongly influenced by the variation of q. In fact, an its increase leads to a very high displacement ductility demand μ. In addition, $\mu_{\ln}(\mu)$ highly decreases by decreasing T_b but is higher for lower values of I_d, especially for high values of T_b.

The IDA results of the isolation level and of the superstructure for the softening behavior are not reported because the influence of the data related to the dynamic collapses has been taken

into account within the assessment of the seismic fragility, as discussed in the next section, together with the description of the influence of the other structural properties (i.e., γ_s, q and S) on both the DFPS and the softening superstructures.

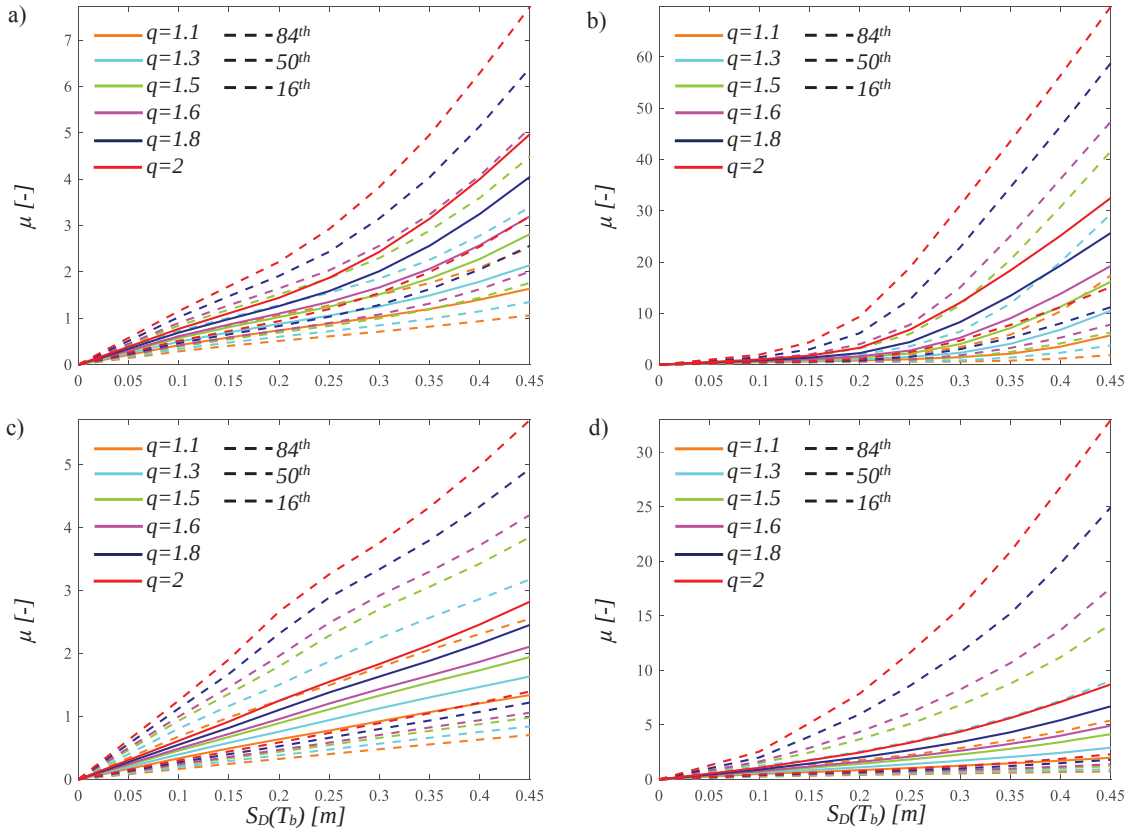

Figure 3: IDA curves of the superstructure with γ_s=0.6 for I_d=2, T_b=3 s, H=0.03 (a), I_d=2, T_b=6 s, H=0.03 (b), I_d=8, T_b=3 s, H=0.03 (c), I_d=8, T_b=6 s, H=0.03 (d).

4 SEISMIC FRAGILITY CURVES

The definition of the limit states with respect to the EDP is necessary to reach the fragility assessment. In detail, different thresholds, respectively, in terms of the radius in plan for each surface of the DFPS isolator, $r_1[m]$ and $r_2[m]$, and of the displacement ductility for the superstructure, $\mu[-]$, have been selected. In this way, the probabilities P_f exceeding the different limit states at each *IM* level, have been numerically computed. Tables 1-2 report, respectively, the failure probabilities in 50 years [50] and the corresponding thresholds, related to the *LS*s provided by the codes [21]-[22]: the failure probability in 50 years [13],[50] associated to the collapse limit state [22] for the DFPS; whereas, the failure probability in 50 years [13],[50] associated to the life safety *LS* [22] for the superstructure in compliance with the design.

For each structural system of the 768 equivalent 3dof systems, the probabilities P_f exceeding the different limit states at each *IM* level, are numerically computed and successively fitted through lognormal distributions [14] with a R-square value higher than 0.8. For the softening systems, the number of both the collapse cases has been considered to estimate the seismic fragility through the total probability theorem [29],[51], as follows:

$$P_{SL}(IM = im) = (1 - F_{EDP|IM=im}(LS_{EDP})) \cdot \frac{N_{not-collapse}}{N} + 1 \cdot \left(1 - \frac{N_{not-collapse}}{N}\right) \quad (15)$$

where N is the overall number of analyses at each IM level, and $N_{not-collapse}$ is the number of numerical simulations without any collapse.

Figures 6-8 depict the fragility curves for increasing IM regarding both softening and hardening structures. Precisely, the curves related to the different structural properties and only to some limit state thresholds ($LS_{r,4}$ and $LS_{\mu,3}$) and to I_d=8 and T_b=3s, are illustrated.

Generally, the seismic fragility is lower for increasing the corresponding limit state threshold and is the highest for the post-yield softening behavior.

Figure 4 illustrates the fragility curves regarding the overall response of isolation level for hardening models.

Figures 6-7 depict the fragility curves of the two surfaces of DFPS for the softening systems.

For the all limit states, P_f decreases slightly for increasing γ_s. Then, especially for high limit state thresholds, the fragility increases by increasing T_b, I_d and decreasing q. Note that the probability exceeding a limit state is quite low for the single surface, with a lower probability for the surface 2 characterized by a lower friction coefficient with a lower radius of curvature, in compliance with the IDA results. Obviously, higher values are achieved for the softening behaviour.

The fragility curves for the nonlinear superstructures are shown in Figures 5 (hardening) and 8 (softening). The exceeding probabilities are slightly lower as γ_s decreases but highly increase for increasing values of q. Conversely, lower values of T_b for fixed I_d lead to an increase of the seismic fragility because a decrease of the period T_s means a decrease of the correlated yielding displacement as well as lower values of T_b for fixed I_d lead to higher values of the seismic fragility. In fact, the coupling between I_d and T_b influences T_s and the associated yielding displacement and so, as also discussed in [28]-[29], with reference to systems with low T_s, the ensuing dynamic amplification can negatively affect the superstructure responses increasing the seismic fragility.

	$LS_{r,1}$	$LS_{r,2}$	$LS_{r,3}$	$LS_{r,4}$	$LS_{r,5}$	$LS_{r,6}$	$LS_{r,7}$	$LS_{r,8}$	$LS_{r,9}$	$LS_{r,10}$
r_i *[m] for i =1,2*	0.05	0.1	0.15	0.2	0.25	0.3	0.35	0.4	0.45	0.5
p_f=1.5·10^{-3} in 50 years										

Table 1: Limit state thresholds for the two surfaces of the DFPS with the associated exceeding probability.

	$LS_{\mu,1}$	$LS_{\mu,2}$	$LS_{\mu,3}$	$LS_{\mu,4}$	$LS_{\mu,5}$	$LS_{\mu,6}$	$LS_{\mu,7}$	$LS_{\mu,8}$	$LS_{\mu,9}$	$LS_{\mu,10}$
μ *[-]*	1	2	3	4	5	6	7	8	9	10
p_f =2.2·10^{-2} in 50 years										

Table 2: Limit state thresholds in terms of μ with the associated exceeding probability.

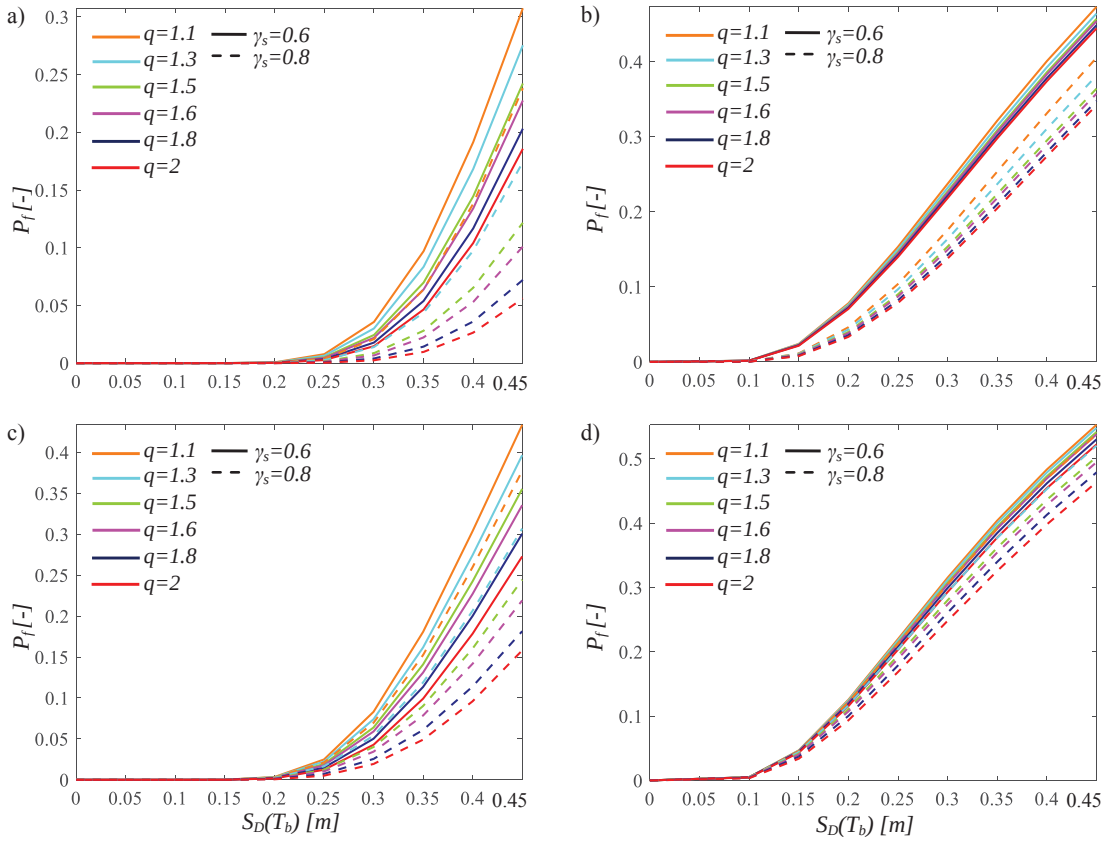

Figure 4: Seismic fragility of the isolation level corresponding to $LS_{r,4}$=0.2 m, for I_d=2, T_b=3 s, H=0.03 (a), I_d=2

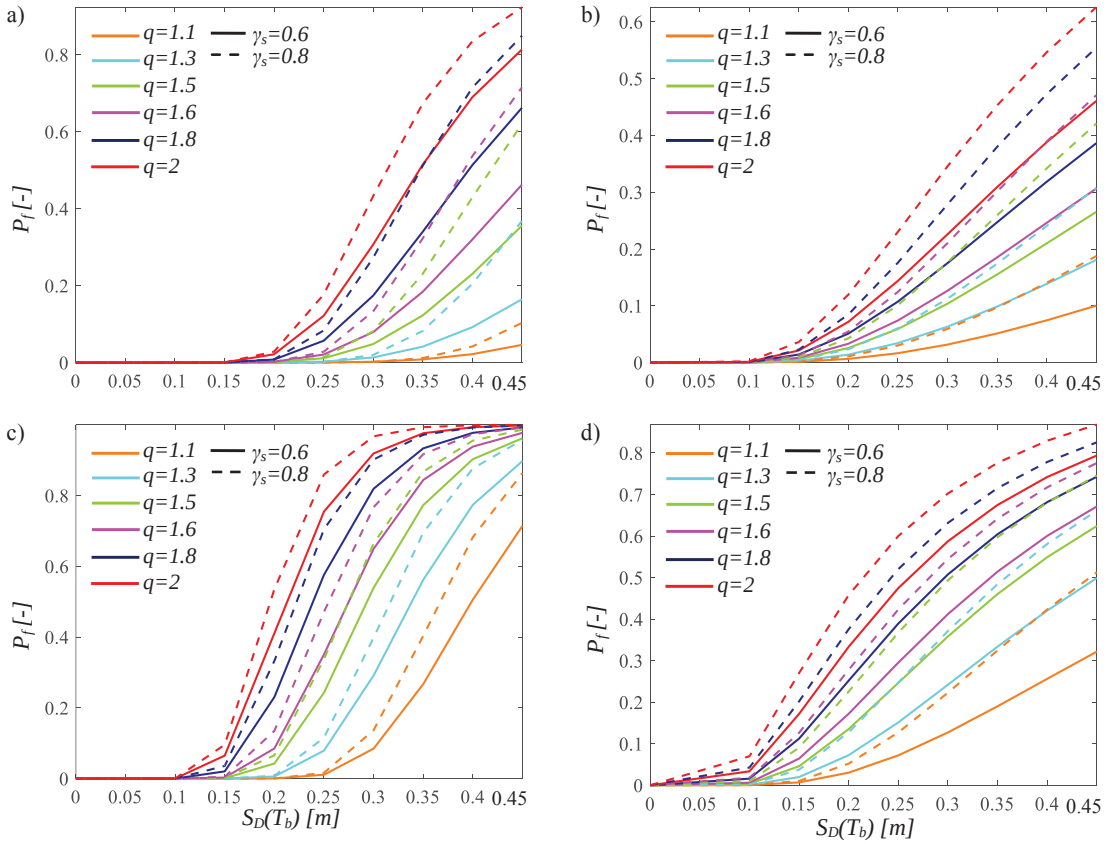

Figure 5: Seismic fragility of the superstructure corresponding to $LS_{u,3}$=3, for I_d=2, T_b=3 s, H=0.03 (a), I_d=2 and T_b=6 s, H=0.03 (b), I_d=8 and T_b=3 s, H=0.03 (c), I_d=8 and T_b=6 s, H=0.03 (d).

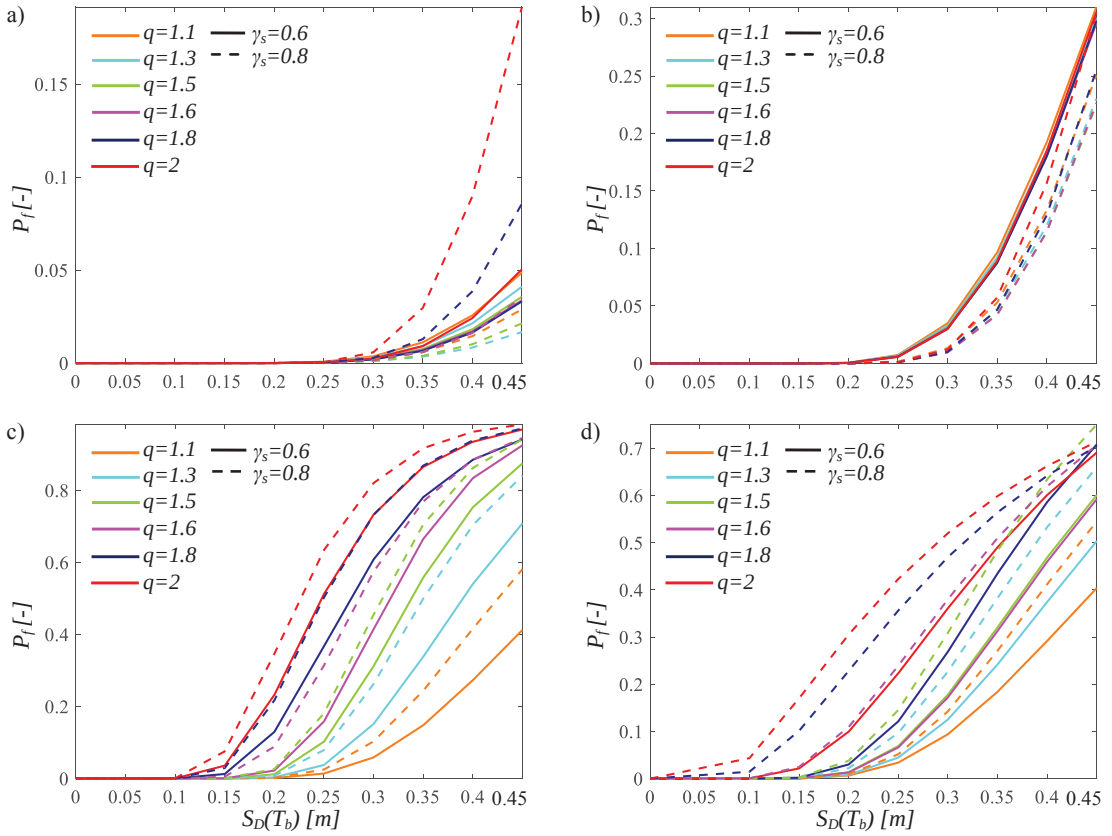

Figure 6: Seismic fragility of the sliding surface 1 corresponding to $LS_{r,4}$=0.2 m, for I_d=2, T_b=3 s, S=0.03 (a),

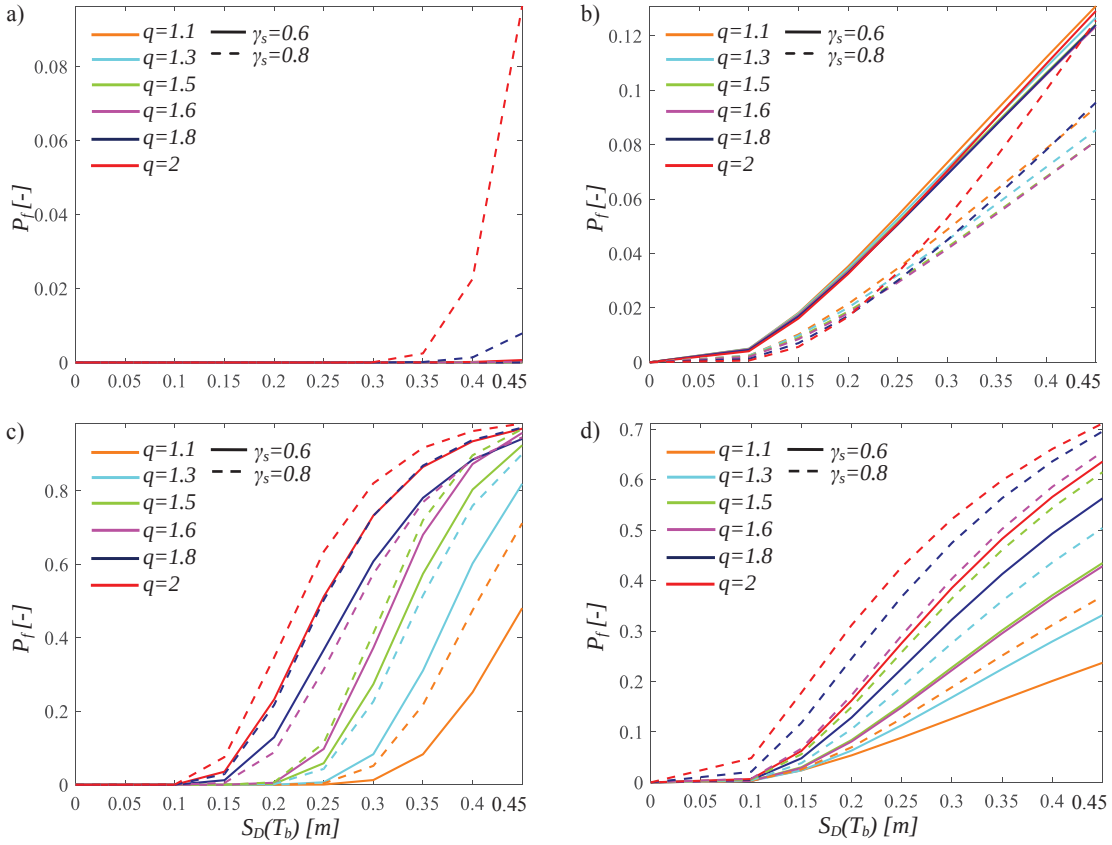

Figure 7: Seismic fragility of the sliding surface 2 corresponding to $LS_{r,4}$=0.2 m, for I_d=2, T_b=3 s, S=0.03 (a), I_d=2 and T_b=6 s, S=0.03 (b), I_d=8 and T_b=3 s, S=0.03 (c), I_d=8 and T_b=6 s, S=0.03 (d).

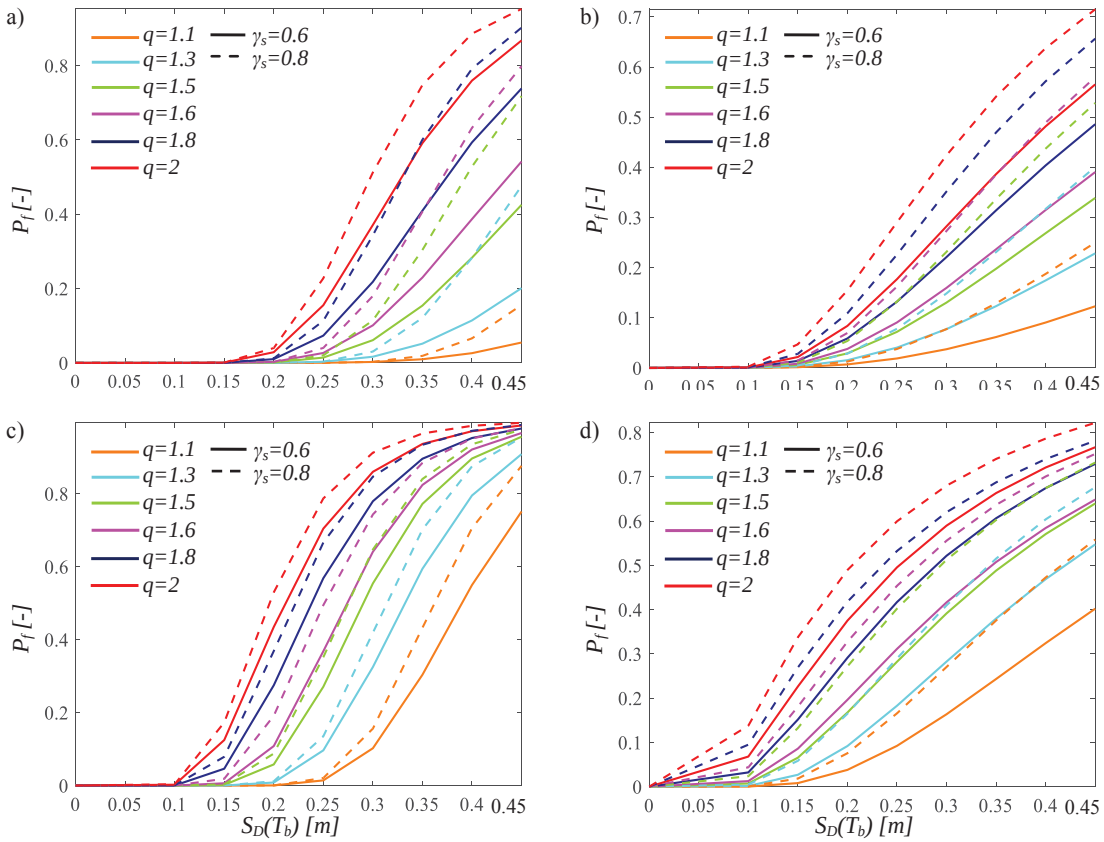

Figure 8: Seismic fragility of the superstructure corresponding to $LS_{\mu,3}=3$, for I_d=2, T_b=3 s, S=0.03 (a), I_d=2 and T_b=6 s, S=0.03 (b), I_d=8 and T_b=3 s, S=0.03 (c), I_d=8 and T_b=6 s, S=0.03 (d).

5 SEISMIC RELIABILITY-BASED DESIGN CURVES FOR DFPS

This section illustrates the results of the seismic reliability assessment for all the equivalent softening or hardening structures isolated by DFPS within their lifetime of 50 years. This assessment is composed of the following two steps: (i) computation of the convolution integral between the seismic fragility curves and the seismic hazard curves, expressed in terms of the same $IM=S_D(T_b)$ [22],[29], to assess the mean annual rates exceeding the limit states; (ii) assessment of the probabilities exceeding the limit states in 50 years through the homogenous Poisson model.

As regards the DFPS isolators, the seismic reliability curves can be seen as the SRBD curves to design the dimensions in plan of each surface and the overall dimension of these devices depending on the expected reliability target and of the structural properties. Figures 9-10 show, respectively, the linear regressions, representative of the seismic reliability of the overall dimension of the isolation level, in the semi-logarithmic space for hardening and softening structures. The R-square value is higher than 0.8. The figures demonstrate that the seismic reliability of the isolation level decreases for the softening behavior in comparison to the hardening case. The increasing direction of the structural parameter q is denoted by means of the arrow in the figures. As for hardening models, these curves demonstrate that an exceeding probability of $P_f=1.5\cdot10^{-3}$ (corresponding to the collapse limit state in 50 years) [50]-[52] requires a global dimension ranging from about 0.3 m to about 1 m depending on the structural characteristics. Instead, for softening superstructures, higher values are required.

Figures 11-22 show the seismic reliability curves for the hardening and softening superstructures highlighting the great influence of the behavior factor as well as the great contribution of the hardening properties in comparison to the softening ones.

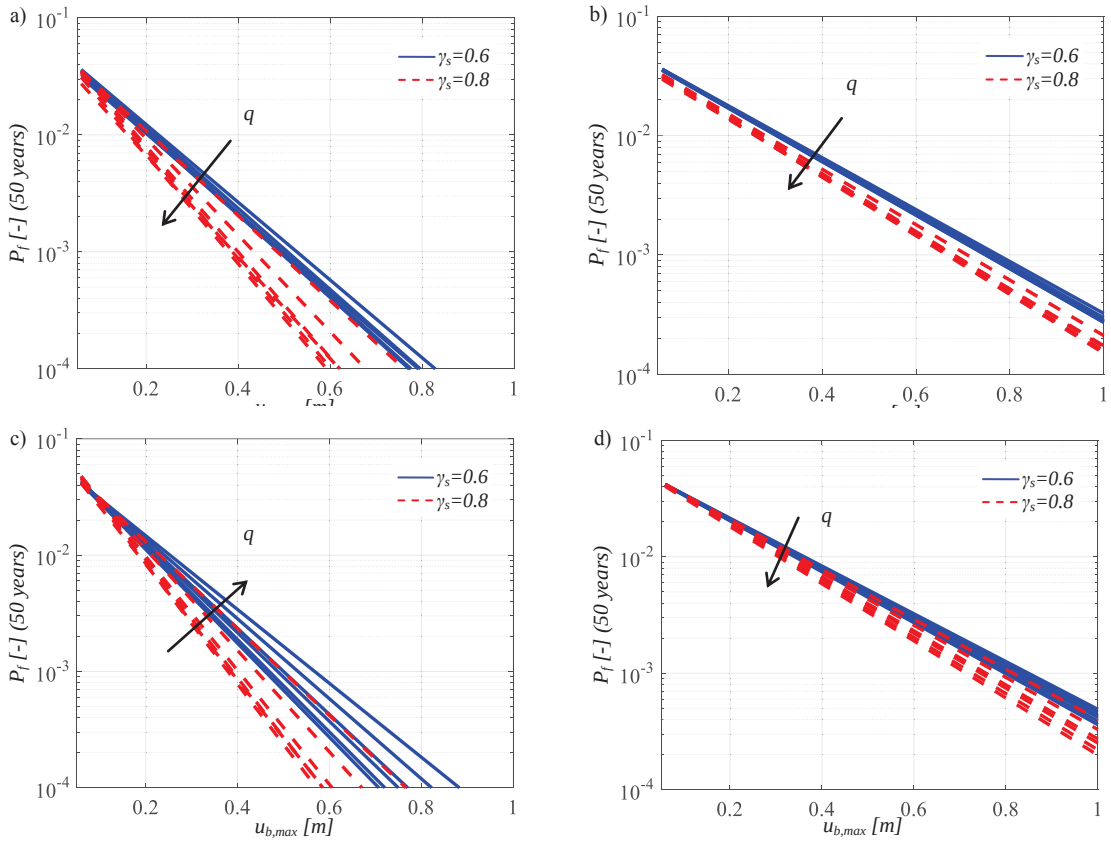

Figure 9: Seismic reliability of the isolation level related to I_d=2, T_b=3 s, H=0.03 (a), I_d=2 and T_b=6 s, H=0.03 (b), I_d=8 and T_b=3 s, H=0.03 (c), I_d=8 and T_b=6 s, H=0.03 (d).

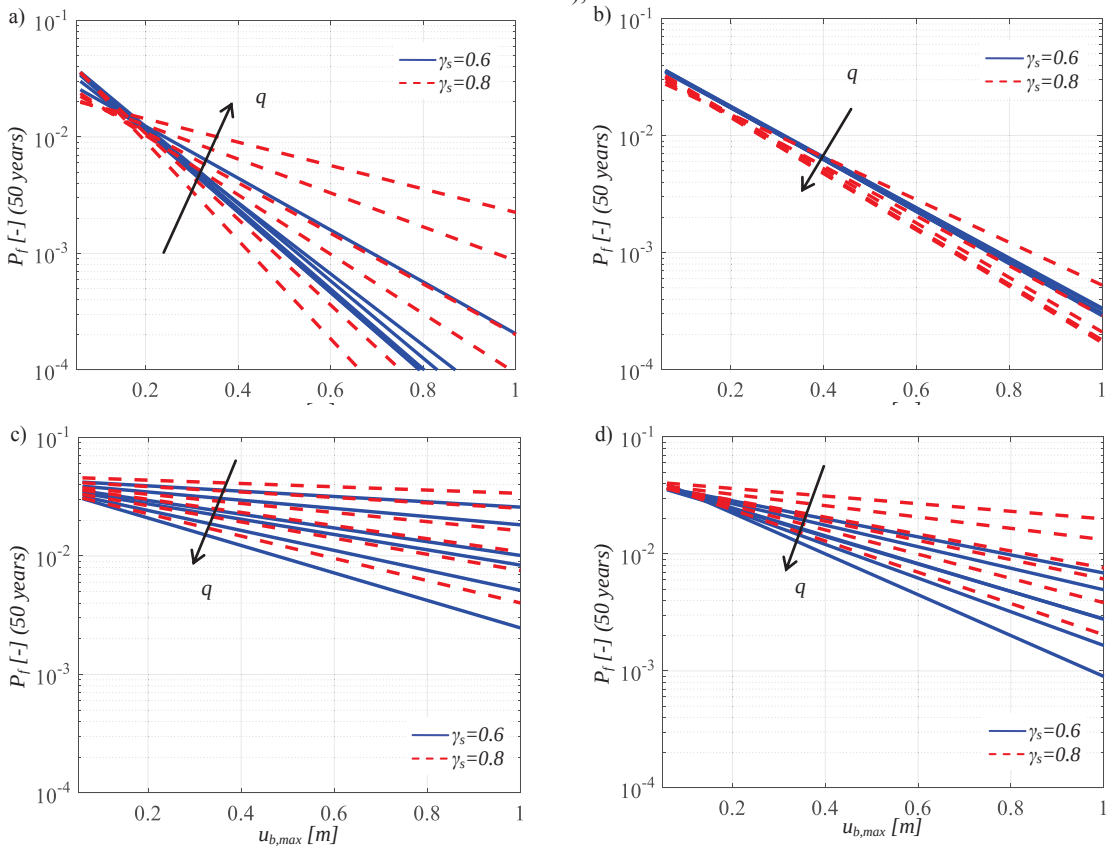

Figure 10: Seismic reliability of the isolation level related to I_d=2, T_b=3 s, S=0.03 (a), I_d=2 and T_b=6 s, S=0.03 (b), I_d=8 and T_b=3 s, S=0.03 (c), I_d=8 and T_b=6 s, S=0.03 (d).

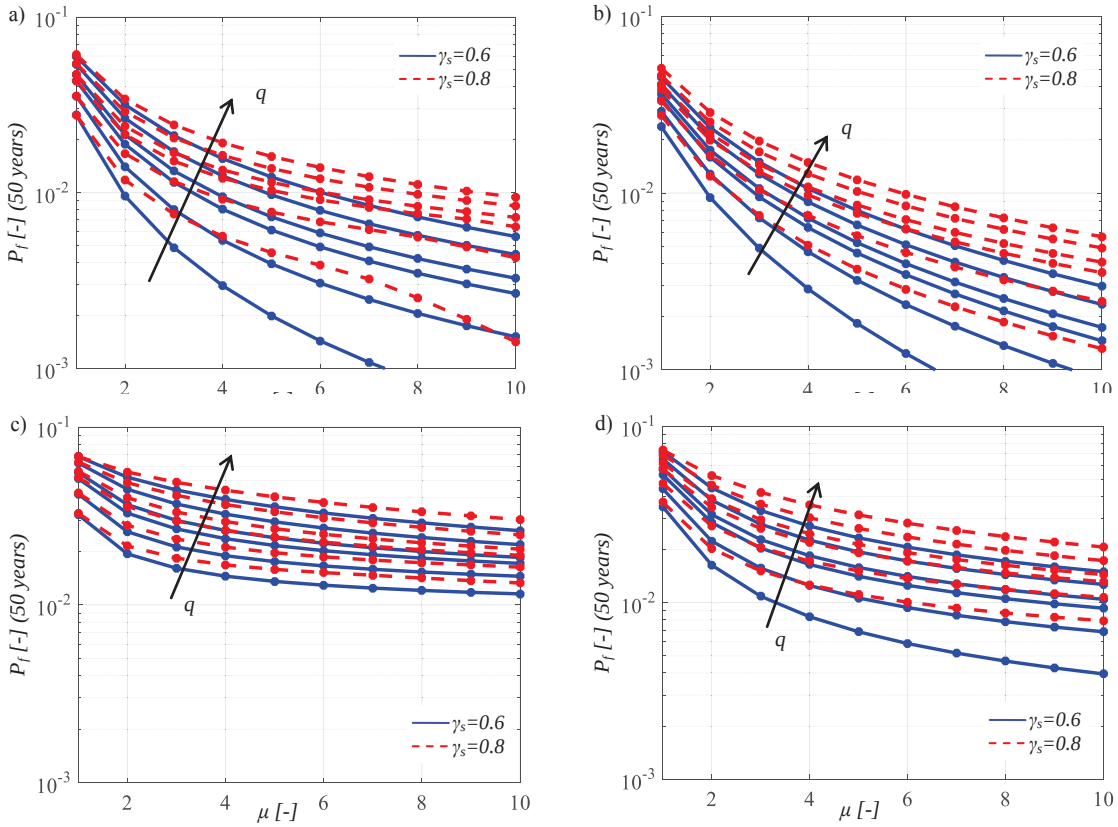

Figure 11: Seismic reliability of the superstructure corresponding to I_d=2, T_b=3 s, H=0.03 (a), I_d=2 and T_b=6 s, H=0.03 (b), I_d=8 and T_b=3 s, H=0.03 (c), I_d=8 and T_b=6 s, H=0.03 (d).

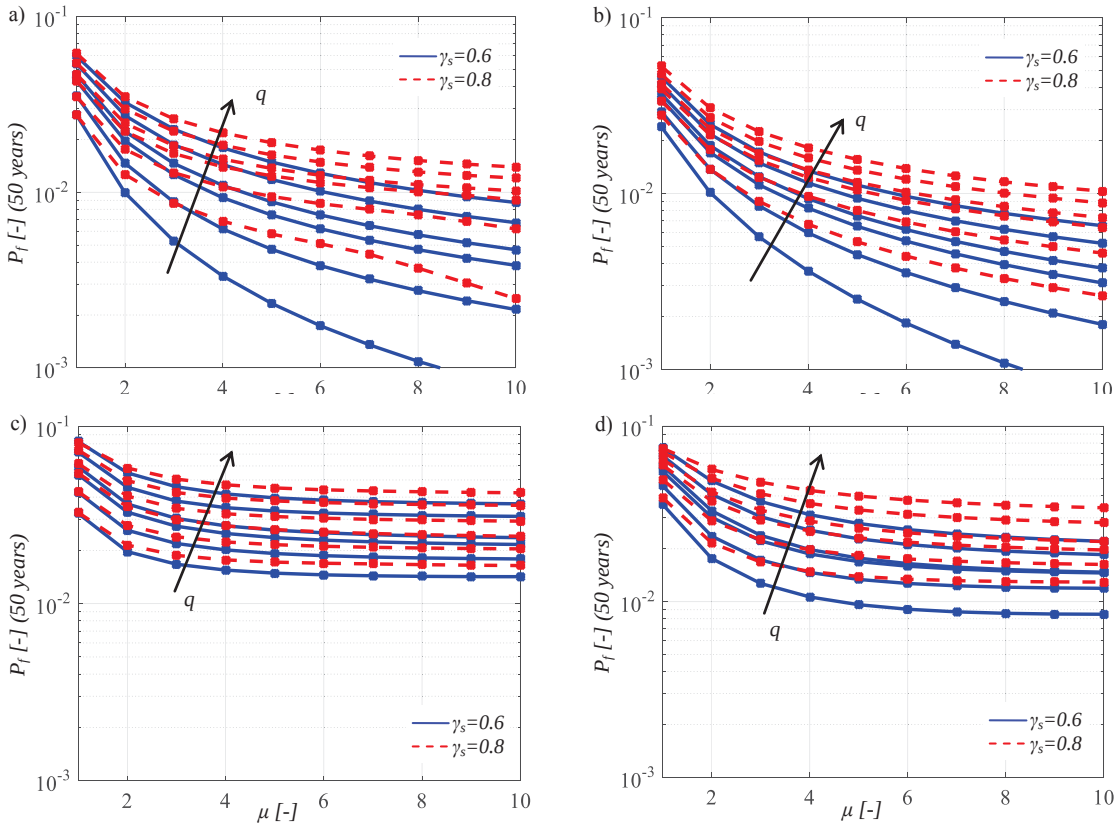

Figure 12: Seismic reliability of the superstructure corresponding to I_d=2, T_b=3 s, S=0.03 (a), I_d=2 and T_b=6 s, S=0.03 (b), I_d=8 and T_b=3 s, S=0.03 (c), I_d=8 and T_b=6 s, S=0.03 (d).

6 CONCLUSIONS

This study focuses on the seismic reliability-based response of hardening and softening structures isolated with double concave sliding isolators. A wide investigation is presented considering different elastic and inelastic mechanical properties and assuming the friction coefficients together with the characteristics of the seismic ground motions as random variables. Adopting an equivalent 3dof system with non-linear velocity-dependent rules for the two surfaces of the DFPS, incremental dynamic analyses are carried out for several natural seismic records, different behavior factors and post-yield stiffness ratios. Then, the seismic fragility curves are derived for each engineering demand parameters of interest for these systems: peak values of the response of the superstructure, of the upper surface and of the lower surface of the DFPS. Successively, assuming a lifetime of 50 years and the seismic hazard of L'Aquila (Italian site), seismic reliability-based design curves are derived for the DFPS. The results have highlighted the great influence of the behavior factor as well as the negative effects of the post-yield stiffness also regarding the seismic reliability of the superstructure.

REFERENCES

[1] C. Christopoulos, A. Filiatrault, Principles of Passive Supplemental Damping and Seismic Isolation. IUSS Press: Pavia, Italy, 2006.

[2] VA. Zayas, SS. Low, SA. Mahin, A simple pendulum technique for achieving seismic isolation. *Earthquake Spectra* 1990; 6:317–33.

[3] L. Su, G. Ahmadi , IG. Tadjbakhsh, Comparative study of base isolation systems. *Journal of Engineering Mechanic* 1989; 115:1976–92.

[4] A. Mokha , MC. Constantinou, AM. Reinhorn, Teflon Bearings in Base Isolation. I: Testing. *J. Struct. Eng.* 1990; 116(2): 438-454.

[5] MC. Constantinou, A. Mokha, AM. Reinhorn, Teflon Bearings in Base Isolation. II: Modeling. *J. Struct. Eng*. 1990; 116(2):455-474.

[6] Troisi R., Alfano G. 2019. Towns as Safety Organizational Fields: An Institutional Framework in Times of Emergency. *Sustainability*, 11: 7025, 2019, doi:10.3390/su11247025.

[7] Troisi R., Alfano G. 2020. Firms'crimes and land use in Italy. An exploratory data anlysis. New Metropolitan Perspectives, International Symposium – 4th edition, 27-30 May 2020, pp 10.

[8] BM. Ayyub, RH. McCuen, Probability, statistics, and reliability for engineers. 2nd ed. NY: CRC Press; 2002.

[9] YK. Lin, GQ. Cai, Probabilistic structural dynamics—advanced theory and applications. NY: McGraw-Hill; 1995.

[10] J. Chen, W. Liu, Y. Peng, J. Li, Stochastic seismic response and reliability analysis of base-isolated structures. *J Earthquake Eng* 2007;11:903–24.

[11] SK. Mishra, BK. Roy, S. Chakraborty, Reliability-based-design-optimization of base isolated buildings considering stochastic system parameters subjected to random earth-

quakes. *Int J Mech Sci* 2013;75:123–33.

[12] P. Castaldo, B. Palazzo, P. Della Vecchia, (2014) Seismic reliability analysis of base-isolated structures with friction pendulum system, EESMS 2014 - 2014 IEEE Workshop on Environmental, Energy and Structural Monitoring Systems, Proceedings, 6923276, 114-119.

[13] P. Castaldo, B. Palazzo, P. Della Vecchia, Life-cycle cost and seismic reliability analysis of 3D systems equipped with FPS for different isolation degrees, *Engineering Structures*, 2016, 125:349–363, http://dx.doi.org/10.1016/j.engstruct.2016.06.056.

[14] P. Castaldo, G. Amendola, B. Palazzo , Seismic fragility and reliability of structures isolated by friction pendulum devices: Seismic reliability-based design (SRBD), *Earthquake Engineering and Structural Dynamics*, 2017, 46(3); 425–446, DOI: 10.1002/eqe.2798.

[15] P. Castaldo, M. Ripani, Optimal design of friction pendulum system properties for isolated structures considering different soil conditions, *Soil Dynamics and Earthquake Engineering*, 2016, 90:74–87, DOI: 10.1016/j.soildyn.2016.08.025.

[16] P. Castaldo, E. Tubaldi, Influence of ground motion characteristics on the optimal single concave sliding bearing properties for base-isolated structures. *Soil Dynamics and Earthquake Engineering*, 2018, 104: 346–364.

[17] YS. Kim, CB. Yun, Seismic response characteristics of bridges using double concave friction pendulum bearings with tri-linear behavior. *Engin. Struct*. 29, 2007, 3082-3093.

[18] P. Castaldo, M. Ripani, R. Lo Piore, Influence of soil conditions on the optimal sliding friction coefficient for isolated bridges. *Soil Dynamics and Earthquake Engineering*, 2018, 111:131–148, https://doi.org/10.1016/j.soildyn.2018.04.056.

[19] CS. Tsai , TC. Chiang, BJ. Chen, Experimental evaluation of piecewise exact solution for predicting seismic responses of spherical sliding type isolated structures. *Earthquake Engineeering and Structural Dynamics*, 2005;34:1027-1046 DOI: 10.1002/equ.430.

[20] Structural Engineering Institute. Minimum design loads for buildings and other structures. Amer. Society of Civil Engineers, 2010.

[21] European Committee for Standardization. Eurocode 8-Design of Structures for Earthquake Resistance. Part 1: General Rules, Seismic Actions and Rules for Buildings, Brussels, 2004.

[22] NTC18. Norme tecniche per le costruzioni. Gazzetta Ufficiale del 20.02.18, DM 17.01.18, Ministero delle Infrastrutture.

[23] Japanese Ministry of Land, Infrastructure and Transport, Notification No. 2009–2000, Tech. Standard for Structural Specif.s and Calculation of Seismically Isolated Buildings 2000.

[24] Quantification of Building Seismic Performance Factors, FEMA P695 / June 2009.

[25] A. Occhiuzzi, D. Veneziano and J. Van Dyck, Seismic design of base isolated structures, Savidis (Ed.), Balkema, Rotterdam, NL.

[26] MD. Mckey, WJ. Conover, RJ. Beckman, A comparison of three methods for selecting values of input variables in the analysis from a computer code. Technometrics 1979;21:239-45.

[27] D. Celarec, M. Dolšek, The impact of modelling uncertainties on the seismic performance assessment of reinforced concrete frame buildings. *Engineering Structures* 2013;52:340–354.

[28] P. Castaldo, B. Palazzo, T. Ferrentino T., Seismic reliability-based ductility demand evaluation for inelastic base-isolated structures with friction pendulum devices, *Earthquake Engineering and Structural Dynamics*, 2017, 46(8): 1245-1266, DOI: 10.1002/eqe.2854.

[29] P. Castaldo, B. Palazzo, G. Alfano, MF. Palumbo, Seismic reliability-based ductility demand for hardening and softening structures isolated by friction pendulum bearings, 2018, *Structural Control and Health Monitoring*, e2256. https://doi.org/10.1002/stc.2256.

[30] Castaldo P., Alfano G. Seismic reliability-based design of hardening and softening structures isolated by double concave sliding devices, *Soil Dynamics and Earthquake Engineering*, 129: 105930, 2020.

[31] HK. Hong, CS. Liu, Internal symmetry in bilinear elastoplasticity, International Journal of Non-Linear Mechanics, 1999, 34:279–288.

[32] GD. Hatzigeorgiou, Ductility demand spectra for multiple near- and far-fault earthquakes. *Soil Dynamics and Earthquake Engineering* 2010;30 170-183.

[33] GD. Hatzigeorgiou, GA. Papagiannopoulos, DE. Beskos, Evaluation of maximum seismic displacements of SDOF systems form their residual deformation. *Engineering Structures* 2011;33 3422-3431.

[34] F. Naeim, KM. Kelly, Design of Seismic Isolated Structures: From Theory to Practice. John Wiley & Sons, Inc.; 1999.

[35] B. Palazzo, Seismic Behavior of base-isolated Buildings. Proc. International Meeting on earthquake Protection of Buildings, Ancona, 1991.

[36] A. Gupta, H. Krawinkler, Seismic demands for performance evaluation of steel moment resisting frame structures. The John A. Blume Earth. Eng. Center report No. 132, June 1999.

[37] C. Adam, LF. Ibarra, H. Krawinkler, Evaluation of P-Delta effects in non-deteriorating MDOF structures from equivalent SDOF systems. *13th Word Conference on Earthquake Engineering*, Vancouver, B.C., Canada 2004, Paper No. 3407.

[38] GD. Hatzigeorgiou, Ductility demand spectra for multiple near- and far-fault earthquakes. *Soil Dynamics and Earthquake Engineering* 2010;30 170-183.

[39] C. Adam, LF. Ibarra, H. Krawinkler, Evaluation of P-Delta effects in non-deteriorating MDOF structures from equivalent SDOF systems. *13th Word Conference on Earthquake Engineering*, Vancouver, B.C., Canada, 2004, Paper No. 3407.

[40] Math Works Inc. MATLAB-High Performance Numeric Computation and Visualization Software. User's Guide. Natick: MA, USA, 1997.

[41] H. Aslani, E. Miranda, Probability-based seismic response analysis. *Engineering Structures* 2005; **27**(8): 1151-1163.

[42] KL. Ryan, AK. Chopra, Estimation of Seismic Demands on Isolators Based on Nonlinear Analysis. *J. Struct. Eng.*, 130(3), 392–402, 2004.

[43] Garzillo C., Troisi R. Le decisioni dell'EMA nel campo delle medicine umane. In EMA e le relazioni con le Big Pharma - I profili organizzativi della filiera del farmaco, G. Giappichelli, 85-133, 2015.

[44] Golzio L. E., Troisi R. The value of interdisciplinary research: a model of interdisciplinarity between legal re-search and research in organizations. *Journal For Development And Leadership*, 2: 23-38, 2013.

[45] Nese A.; Troisi R. Corruption among mayors: evidence from Italian Court of Cassation judgments, *Trends In Organized Crime*, 1-26, 2018. DOI:10.1007/s12117-018-9349-4.

[46] Troisi R., Golzio, L. E. Legal studies and organization theory: a possible cooperation. *Manageable cooperation* - European Academy of Management: 16th EURAM Conference, Paris, 1-2, 1-4 June 2016.

[47] Troisi R., Guida V. Is the Appointee Procedure a Real Selection or a Mere Political Exchange? The Case of the Italian Health-Care Chief Executive Officers. *Journal of Entrepreneurial and Organizational Diversity*, 7 (2): 19-38, 2018, DOI:10.5947/jeod.2018.008.

[48] Castaldo, P., Gino, D., Bertagnoli, G. & Mancini, G. Resistance model uncertainty in non-linear finite ele-ment analyses of cyclically loaded reinforced concrete systems, *Engineering Structures*, 211: 110496, 2020, https://doi.org/10.1016/j.engstruct.2020.110496.

[49] P. Castaldo, D. Gino, G. Mancini, Safety formats for non-linear analysis of reinforced concrete structures: discussion, comparison and proposals. *Engineering Structures*, 193,136-153, 2019.

[50] RD. Bertero, VV. Bertero, Performance-based seismic engineering: the need for a reliable conceptual comprehensive approach. *Earthquake Engineering and Structural Dynamics,* 2002;31:627–652 (DOI: 10.1002/eqe.146).

[51] P. Bazzurro, CA. Cornell, N. Shome, JE. Carballo, Three proposals for characterizing MDOF nonlinear seismic response. *Journal of Structural Engineering*, 1998, 124(11), 1281-1289.

[52] CEN – European Committee for Standardization. Eurocode 0: Basis of Structural Design. Final draft. Brussels, 2006.